

## *Supporting Information*

### **Multivariate statistical characterization of charged and uncharged domain walls in multiferroic hexagonal YMnO<sub>3</sub> single crystal visualized by a spherical aberration-corrected STEM**

*By Takao Matsumoto\*, Ryo Ishikawa, Tetsuya Tohei, Hideo Kimura, Qiwen Yao, Hongyang Zhao, Xiaolin Wang, Dapeng Chen, Zhenxiang Cheng, Naoya Shibata, and Yuichi Ikuhara*

#### **Details of the MSA analysis**

Analysis of the ABF images as the one shown in Figure 3, as well as HAADF images simultaneously obtained with the ABF images, were done as follows: First, the whole (1024 pixels x 1024 pixels) HAADF image at a nominal magnification of 8M was divided into five rectangular subimages (Up, Down, LDW, TDW, and Step regions as designated in the figure) according to the apparent directions of polarization which can be evaluated by the characteristic two-up and one-down or two-down and one-up patterns of the Y atomic column positions. In this condition, a pixel corresponds to 0.0182 nm. Then, from the Up HAADF image, a typical subimage (45 pixels x 35 pixels) consisting of four Y and four Mn atomic columns was selected and used as a template for the template matching procedure (cvMatch\_Template plugin for ImageJ) to produce a gallery of 121 subimages. Using the same coordinates as used for the extraction of HAADF subimages, ABF subimages were extracted to produce an image gallery. The PCA analysis in MSA plugin for ImageJ was performed for these image galleries to produce 121 factorial images for each HAADF and ABF gallery. In the following, for simplicity, the same description is applied for each HAADF and ABF image. The first factorial image

corresponds to the average image for the upward polarization. The same procedure was applied for the Down images, and we obtained an average image for the downward polarization. In both analyses, the second factorial images correspond to the variation of images due to various noises originating from statistical noise, beam-scanning noise, and other instabilities of the microscope. Such variations were minimized as expected for the current state-of-the-art microscope technology we've employed. By using the two average image as a template, image galleries for the LDW, TDW, and Step images were obtained and analyzed by MSA procedure. For LDW, TDW and Step images, images corresponding to upward and downward polarization coexist. Therefore, the first factorial image corresponds to the average image between the two polarization while the second factorial image corresponds to the difference between upward and downward polarization. The score images were reconstructed from the average image (the first factorial image) and the difference image (the second factorial image) as linear weighted sum images according to the factorial coordinates. The reconstructed score images were colored according to their second factorial coordinates in such a way that subimages which have the larger component of upward polarization were drawn in deeper red while subimages having the larger component of downward polarization were drawn in thicker light-blue. Finally, all of the reconstructed score images with color were placed back at the original positions in the original image to produce a final color map. Biplots as shown in Figures S1 and S2 were obtained by a macro program running on ImageJ written by T.M. The plots show the distribution of factorial coordinates for each subimage.

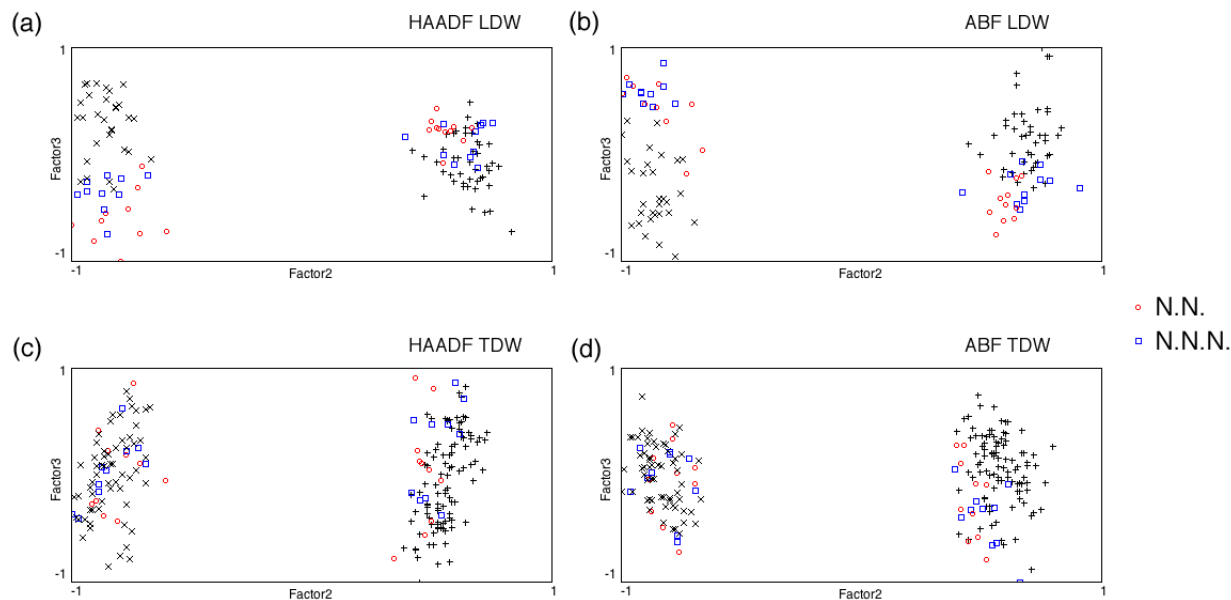


**Figure S1.** Biplots of the MSA coordinates applied to the LDW HAADF (a), LDW ABF (b), TDW HAADF (c), and TDW ABF (d) image gallery. The separation of the two groups are clear, and images corresponding to the nearest neighbor (N.N) and next nearest neighbor (N.N.N.) transition regions are highlighted with red and blue, respectively.

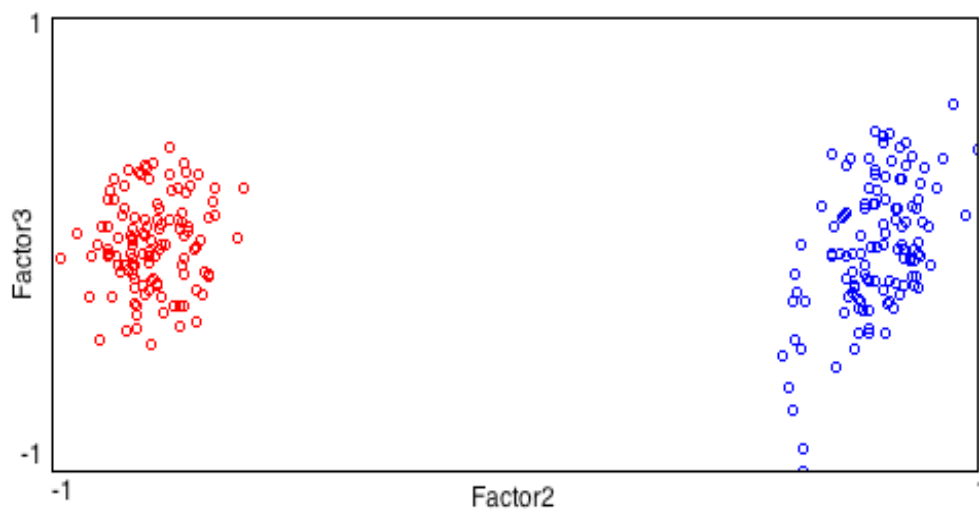


**Figure S2.** A biplot of the MSA coordinates applied to an artificial Up and Down image group created by concatenating the two image galleries.

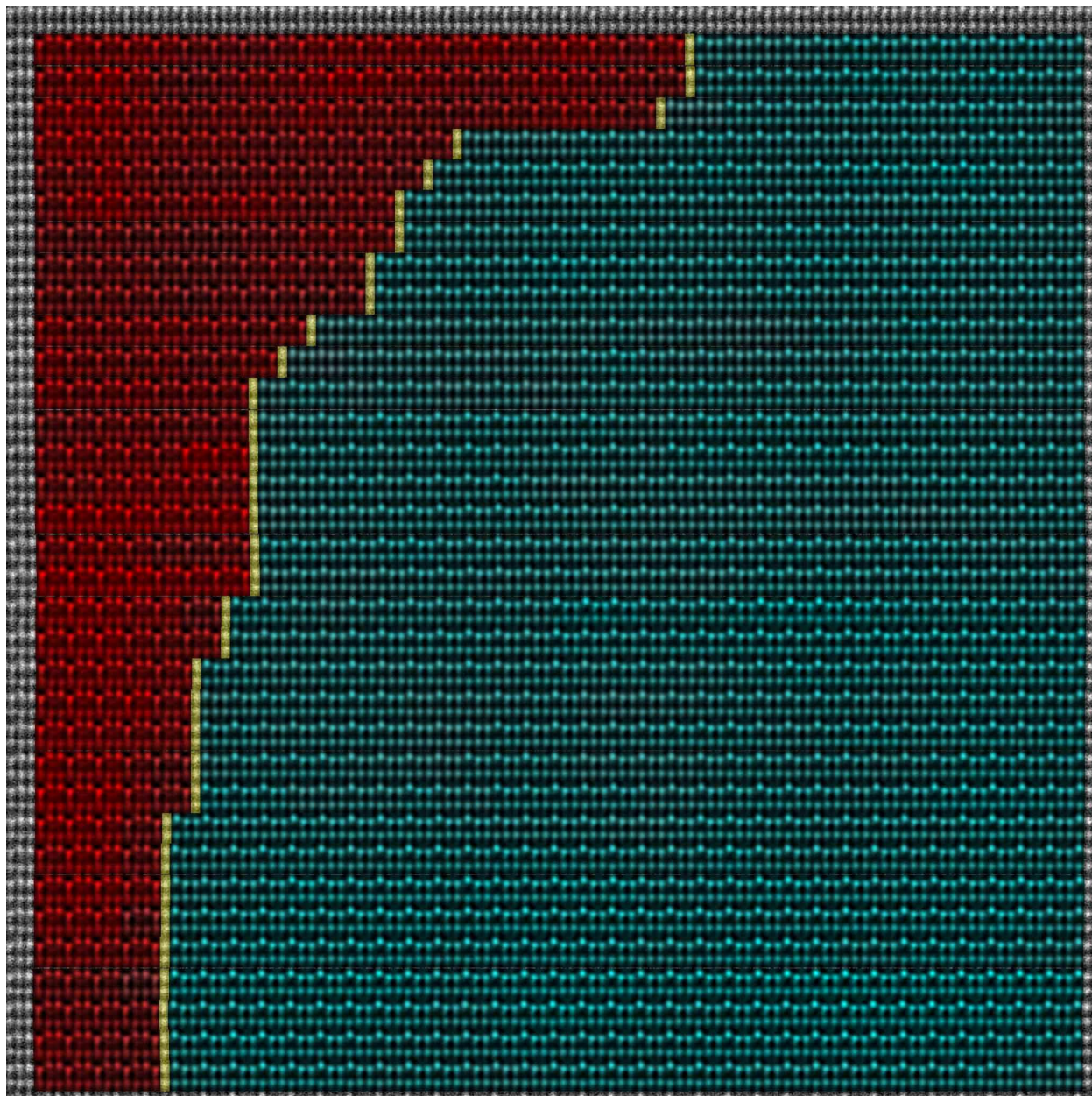


**Figure S3.** A colored MSA reconstructed score image of TDW domain wall with  $2a/3$  displacement. Compared with the TDW domain wall with  $a/3$  displacement, an additional

yellow-colored atomic column is inserted at each boundary. The domain wall with  $a/3$  displacement was observed to be unstable so that the image quality was not so good as the domain wall with  $a/3$  displacement.

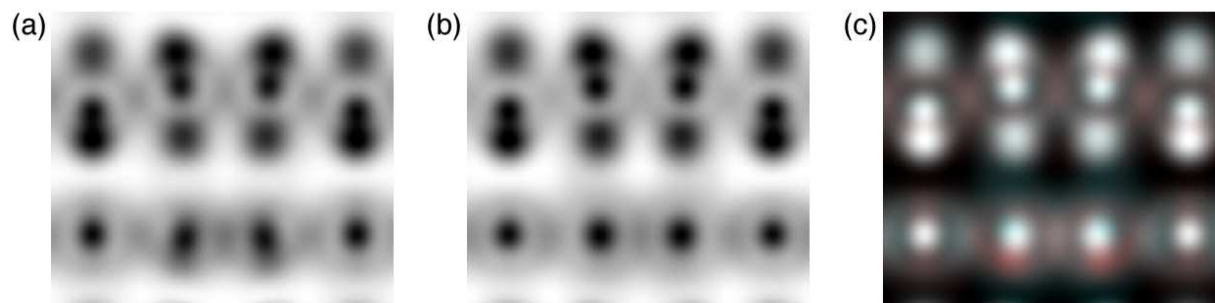


**Figure S4.** Computer simulated ABF images with (a) and without (b) oxygen atoms in the vicinity of Mn layer. The different sites between the two images are highlighted with color (red indicates positive difference while blue indicates negative difference) in (c).

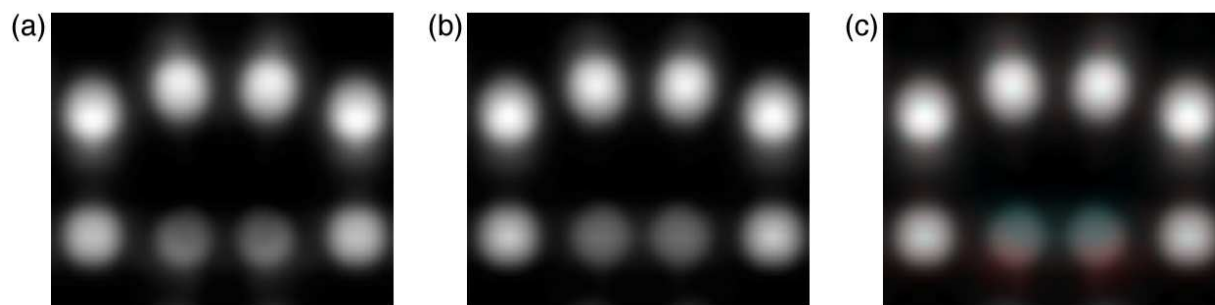


**Figure S5.** Computer simulated HAADF images with (a) and without (b) oxygen atoms in the vicinity of Mn layer. The different sites between the two images are highlighted with color (red indicates positive difference while blue indicates negative difference) in (c).

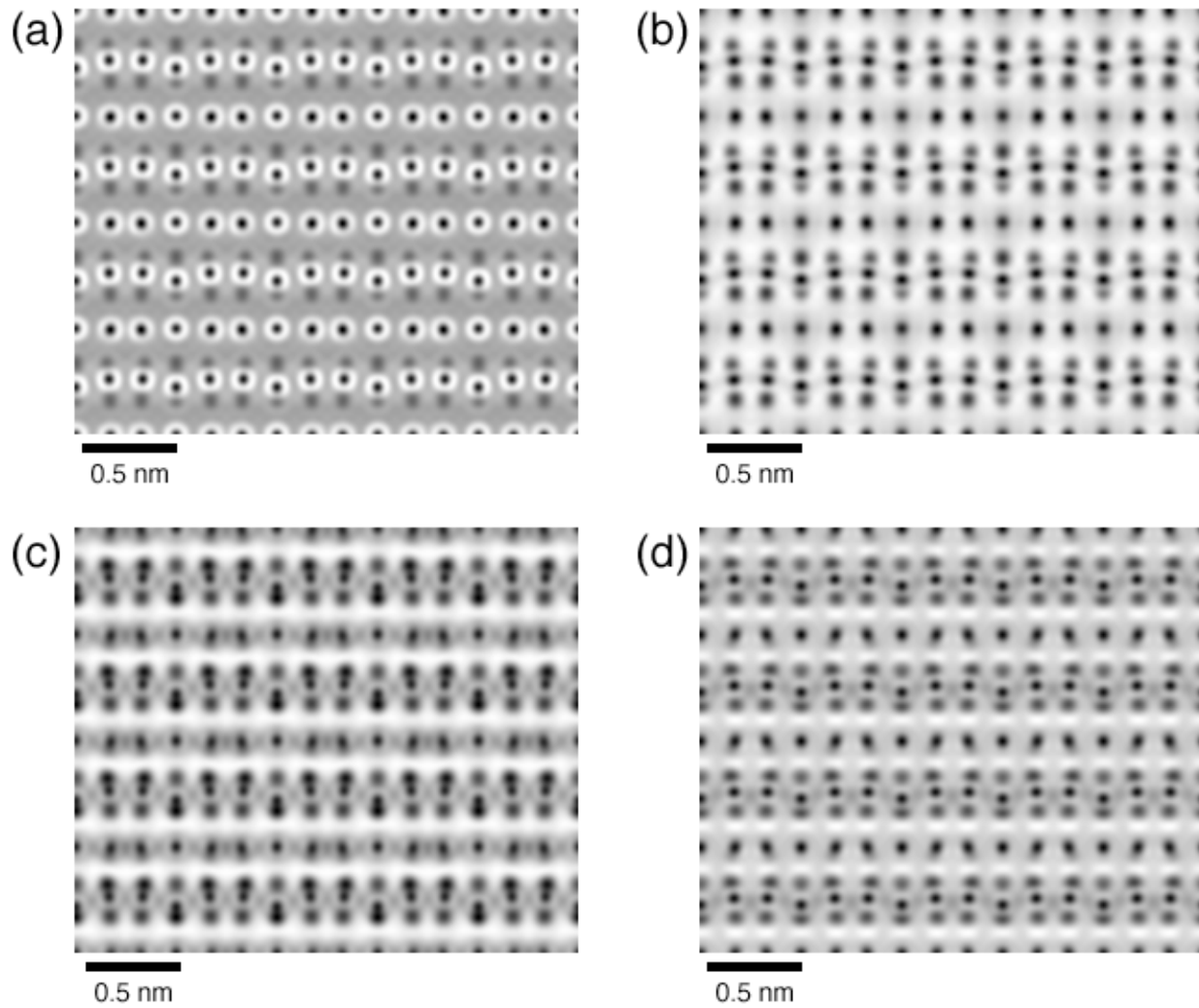


**Figure S6.** Computer simulated ABF images for different specimen thicknesses, (a) 5 nm, (b) 10nm, (c) 20 nm, and (d) 30 nm. All images exhibit the double-arc shape with opposite curvatures for Y layers and Mn-O layers, but the appearance has a slight dependence on the thickness of the thin film.

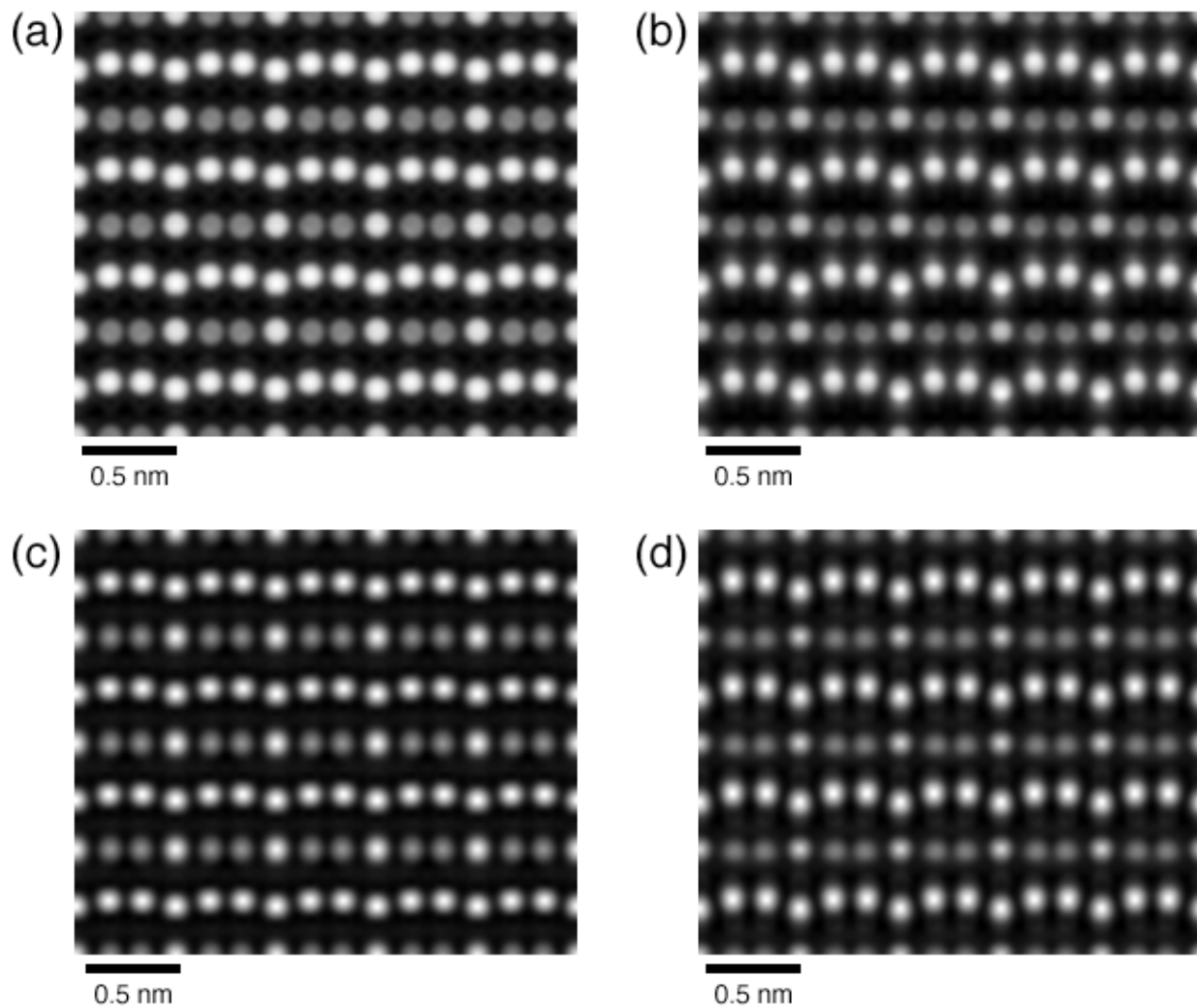


**Figure S7.** Computer simulated HAADF images for different specimen thicknesses, (a) 5 nm, (b) 10nm, (c) 20 nm, and (d) 30 nm. All images exhibit the double-arc shape with opposite curvatures for Y layers and Mn-O layers, but the appearance has a slight dependence on the thickness of the thin film.

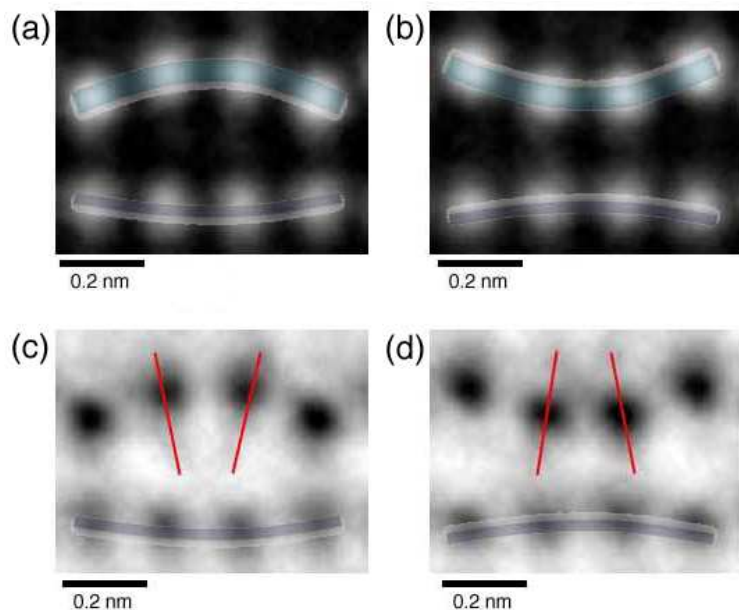


**Figure S8.** Double-arc shapes having opposite curvature revealed in MSA reconstructed HAADF images for (a) upward and (b) downward polarization. The same double-arc shapes are recognized in ABF images for (c) upward and (d) downward polarization. In addition, the angle between the vertical direction (c-axis) and red tilting lines correspond to a projected tilting angle of  $\alpha$  connecting the neighboring oxygen column images (see Figure S9).

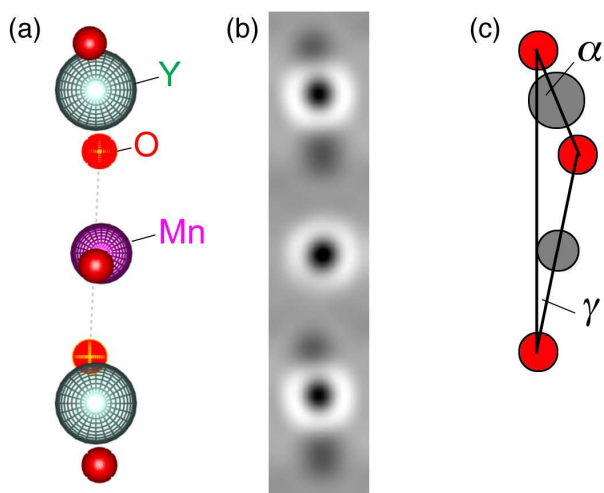


**Figure S9.** An atomic model (a) of  $\text{YMnO}_3$  along  $[110]$  direction focusing on how the tilting of a  $\text{MnO}_5$  bipyramid is reflected in an a corresponding computer simulated ABF image (b). As schematically shown in (c), the projected tilting angle is designated as  $\gamma$ , while a projected tilting angle of  $\alpha$  connecting the neighboring oxygen column images is observed in the vicinity of Y layer. This corresponds to the red tilting line in Figure S8d and S8e.

**Details of the analysis of image shift in individual Y-layer and Mn-O layer in the direction of c-axis as shown in Figures 8 and 9.**

First, each MSA averaged image with a width of 45 pixels and a height of 35 pixels for correspondingly numbered rows has been calculated by using the same method described in **Details of the MSA analysis** in the same document. Then, as illustrated in Figure S10, 10 pixels by 15 pixels region of interest (ROI) is specified for each atomic column A-D independently in either Y or Mn-O layer. The centers of mass in pixels for atomic columns A-D have been estimated by using ImageJ's built-in function as shown in Tables S1 and S2. The relative image shift has been estimated as the average difference between the inner two atomic columns (B and C) and the outer two atomic columns (A and D). Finally, these image shifts in pixels are converted to values in nm.

**Figure S10.** A schematic diagram illustrating the method of analyzing the image shift in Y layer and Mn-O layer.

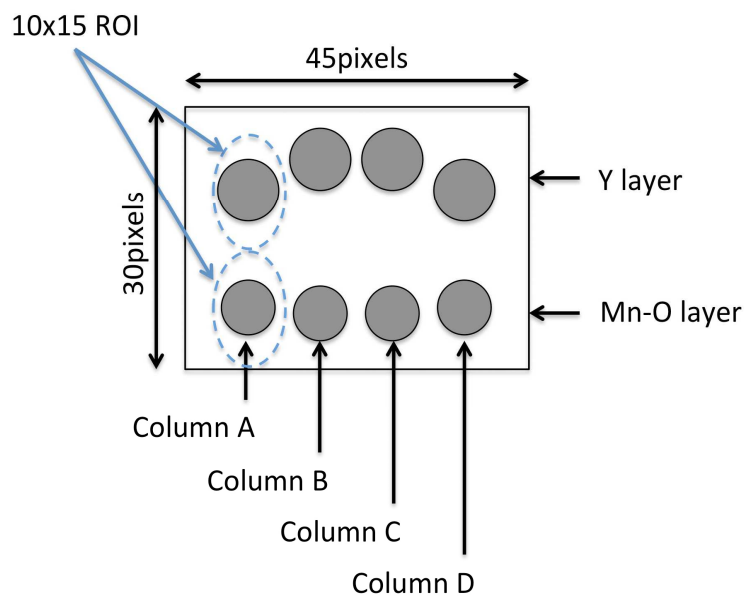


**Table S1. Vertical coordinates of centers of mass of the atomic columns (A-D) for Mn-O layers (Row 0-6) used in LDW analysis, and estimated image shift values**

Row	A [pixel]	B [pixel]	C [pixel]	D [pixel]	$(B+C)/2-(A+D)/2$ [pixel]	Shift [nm]
0	24.275	25.182	25.155	24.318	0.872	0.0158
1	24.398	25.534	25.293	24.394	1.0175	0.0185
2	25.489	26.07	25.777	25.423	0.4675	0.0085
3	24.692	25.1	24.834	24.646	0.298	0.0054
4	25.601	24.9	25.054	25.564	-0.6055	-0.0110
5	25.415	24.227	24.45	25.388	-1.063	-0.0193
6	25.738	24.836	24.997	25.792	-0.8485	-0.0154

**Table S2. Vertical coordinates of centers of mass of the atomic columns (A-D) for Y layers (Row 0-6) used in LDW analysis, and estimated image shift values**

Row	A [pixel]	B [pixel]	C [pixel]	D [pixel]	$(B+C)/2-(A+D)/2$ [pixel]	Shift [nm]
0	10.035	7.165	7.129	10.073	-2.907	-0.0529
1	9.583	6.805	6.823	9.635	-2.795	-0.0508
2	9.483	6.704	6.798	9.463	-2.722	-0.0495
3	9.156	6.639	7.055	9.185	-2.3235	-0.0422
4	6.728	8.56	9.315	6.74	2.2035	0.0401
5	6.684	9.368	9.724	6.649	2.8795	0.0524
6	6.44	9.068	9.212	6.386	2.727	0.0496